Title

Seismogenic Inversion Layer: Depth-dependent Slow Earthquakes Controlled by Temperature Dependence of Brittle-ductile Transitional Rheology

Authors

Ryosuke Ando,[1]* Kohtaro Ujiie,[2] Naoki Nishiyama,[3] Yasushi Mori[4]

Affiliations

[1] Graduate School of Science, University of Tokyo, Tokyo, Japan.

[2] Graduate School of Science and Technology, University of Tsukuba, Tsukuba, Japan

[3] Geological Survey of Japan, National Institute of Advanced Industrial Science and Technology, Tsukuba, Japan

[4] Kitakyushu Museum of Natural History and Human History, Kitakyushu, Japan

Corresponding author: Ryosuke Ando (ando@eps.s.u-tokyo.ac.jp)

Key Points:

- Depth-dependence of slow earthquakes is characterized as the seismogenic inversion layer (SIL); not monotonic brittle-ductile transition
- A simple and general physics-based model is proposed to describe the depth dependence of slow earthquakes with particular attention to SIL
- The key mechanism is the reduction of both the fraction of brittle blocks and viscosity of plastically deformed matrix in fault zones

Abstract

The discovery of slow earthquakes illuminates the existence of a strange depth dependence of seismogenesis, which contradicts the common understanding of smooth brittle/seismic-ductile/aseismic transition as going deeper into the earth's surface layers. However, within the transitional layer on plate interfaces, observations have clarified slip velocities of slow earthquakes changing from those slower to faster with increasing depth, as described by the "seismogenic inversion layer." We propose a new mechanical model that can consistently explain the classic brittle-ductile transition and this inversion phenomenon by considering the heterogeneous fault zone composed of brittle blocks in the ductile matrix. The key mechanism is the interplay between the volumetric fraction of brittle blocks and the viscosity of the surrounding plastically deformed matrix, where the former and the latter decrease with increasing temperature. This model is extended to shallow-slow earthquakes. Our results open a new pathway to infer the deformation mechanisms underlying slow earthquakes.

Plain Language Summary

We have believed that the earth's surface is cold and crispy while the interior is warm and soft, and the crispy layer called the seismogenic layer gradually changes to the soft layer, not generating earthquakes, with going deeper into the earth along plate interfaces. However, recent observations show that this change is not actually gradual. Instead, it involves the layer of the reverse tendency that we call the "Seismogenic Inversion Layer (SIL)" that hosts so-called deep slow earthquakes. To explain this enigmatic phenomenon, we propose a simple mechanical model based on the fundamental laws of rock physics. We find the key mechanism that generates SIL is the change in the rock property depending on the temperature inside the earth. Given rocks are composed of relatively crispy parts and soft parts, SIL is explained only if we consider the crispy parts shrink and the soft parts become softer with increasing temperature and depth.

1. Introduction

The depth dependence of the slow earthquakes has become established with some localities [*Frank et al.*, 2015; *Obara*, 2011; *Shelly and Johnson*, 2011; *Wech et al.*, 2009], but the underlying mechanism is poorly understood. Figure 1a and Table 1 summarize the observed depth-dependent features, presenting significantly different modes of slow earthquakes. Below the regular seismogenic depth, the modes of slow earthquakes are changed from long-term slow slip events (L-SSEs), short-term SSEs (S-SSEs) and tremors [*Obara*, 2011; *Wech et al.*, 2009]. We call them deep-slow earthquakes that occur

down-dip of the seismogenic zone, contrasted with shallow-slow earthquakes up-dip of the seismogenic zone. The L-SSEs are much slower and larger slip or stress release events in the durations of months to years [*Miyazaki et al.*, 2006] with less seismic radiation[*Frank et al.*, 2015] than S-SSEs in the durations of weeks to a month [*Hirose and Obara*, 2005; *Rogers and Dragert*, 2003]. Interestingly, L-SSEs are typically found in the Nankai (Japan) [*Kobayashi*, 2017] and Guerrero (Mexico) [*Frank et al.*, 2015] subduction zones. While L-SSEs are yet to be found in the transform fault such as the San Andreas fault (USA) and the Cascadia (USA/Canada) subduction zone, the slip there may be more steady in the corresponding depth range[*Michel et al.*, 2019]. Below the depth of L-SSEs and after-slips [*Shelly and Johnson*, 2011], the area of S-SSEs exists as overlapped with the tremor area [*Obara*, 2011], as often called episodic tremor and slip (ETS). Further, detailed observations show that the peak of the slip amount is located at a shallower depth than that of the tremor generation during an ETS episode [*Wech et al.*, 2009].

These observations illuminate the existence of the enigmatic depth range, which is characterized by the peak of the slip speed within the transition zone, as schematically illustrated in Figure 1a. This depth range may be called "the seismogenic inversion layer (SIL)." As noted previously [*Scholz*, 1998], the existence of this peak at the intermediate depth contradicts our expectation from the monotonic transition of the frictional instability from the seismogenic (velocity-weakening) shallow layer to the aseismic (velocity strengthening) deep layers, as often described by the negative to the positive transition of the $(a - b)$ value invoking the rate- and state-dependent friction [*Liu and Rice*, 2007; *Tse and Rice*, 1986] (Figure 1b). Available physics-based models for slow earthquakes [*Ando et al.*, 2012; *Liu and Rice*, 2007; *Matsuzawa et al.*, 2013; *Segall et al.*, 2010; *Skarbek et al.*, 2012] are yet to identify the intrinsic mechanism of the depth-dependent slow earthquake modes or the origin of SIL. Qualitative geological models, attributing the slab dehydration [*Hyndman et al.*, 2015] and the mantle-wedge structure [*Katayama et al.*, 2012], are limited to specific subduction zone conditions.

Notably, the abovementioned characterization appears to be applicable as independent of tectonic settings, whether a transform fault [*Shelly and Johnson*, 2011; *Wech et al.*, 2012], or the subduction interfaces [*Obara*, 2011; *Wech et al.*, 2009]. The conditions of fault zone materials would be different in these plate interfaces, as summarized in Supplementary Table 1. Petrological studies suggest that slow earthquakes are independent of specific metamorphic reactions, considered the presumed higher temperature range in Cascadia than Nankai [*Peacock*, 2009]. The depth-dependent features have been interpreted regarding the material discontinuity with Moho [*Obara*,

2011] and the subduction dehydration and fluid migration [*Hyndman et al.*, 2015]. However, the above observations show the universal depth-dependence; this motivates us to explore a more general primary control rather than those specific to the tectonic settings, mineral compositions and metamorphisms.

This study seeks the primary controlling factor of the depth-dependent slow earthquakes by focusing on the most basic rheological property of subduction-related mélange shear zones: the dependence on the ambient temperature. Well examined are the positive temperature dependences of the frictional velocity-dependence ($a - b$) [*Blanpied et al.*, 1995; *Scholz*, 2019] and the negative dependence of the viscosity of the rock plasticity [*Karato*, 2008], respectively (Figure 1b). However, their properties in the transition zone have no consensus, while geological examples suggest the importance of the mixed brittle and ductile components [*Burgmann*, 2018; *Fagereng et al.*, 2014]. To unify the geological and geophysical observations, we construct and analyze a physics-based model with the rheological heterogeneity of brittle patches in the ductile matrix [*Ando et al.*, 2012]. The key ingredient of our model is the temperature effect on the rock viscosity and the brittle over ductile fraction in the mélange shear zones (Figure 1c).

2 Modeling and analysis method

2.1 Geological observation

We begin by developing our geological picture of mélange shear zones at the brittle-ductile transition depths. Figure 2a shows an example of a block-in-matrix structure that is developed in the Nishikashiyama mélange deformed at the pressure of ~1.0 GPa and the temperature of ~500 ºC under epidote-amphibolite facies metamorphic condition [*Mori et al.*, 2014; *Tulley et al.*, 2022; *Ujiie et al.*, 2022]. The Nishikashiyama mélange is marked by competent blocks of metabasite and metapelite in the chlorite-actinolite schist (CAS) matrix that is considered to originate from mechanical mixing and chemical reactions between serpentinite and metabasite near the mantle wedge corner [*Mori et al.*, 2014; *Nishiyama*, 1989; 1990]. The matrix foliation is defined by the alignment of chlorite and actinolite, commonly showing asymmetric fabrics such as S-C fabric with their shear sense consistent with megathrust shear (Figure 2a) [*Tulley et al.*, 2022; *Ujiie et al.*, 2022]. The recent quartz grain-size piezometry and quartz flow law analyses indicated the CAS matrix recorded an increase in strain rate of ~10^{-10} s^{-1}, which may be comparable to slow slip strain rates [*Ujiie et al.*, 2022]. The stability field of chlorite and actinolite [*Hacker et al.*, 2003] (Figure 2b) suggests that the assemblage of chlorite-actinolite is likely ubiquitous along plate interfaces, including the P-T range of

the ETS zones [*Peacock*, 2009]. We presume that the observed block-in-matrix structure in the Nishikashiyama mélange represents heterogeneous shear zones at source regions of ETS (Figure 1c). Such heterogeneity was also reported not only from the subduction zone setting [*Behr et al.*, 2018; *Fagereng et al.*, 2014; *Ujiie et al.*, 2018] but also from the crustal/transform fault setting [*Scholz*, 2019; *Sibson*, 1977]. There, the brittle (or yield)-strength can emerge from stress chains supported by the blocks (Figure 2c, top), and the ductile strength becomes effective due to the matrix flow once the stress chains collapse during slip events (Figure 2c, bottom), as in granular experiments [*Boyer et al.*, 2011; *Howell et al.*, 1999].

2.2 Mechanical model

We next develop a new mechanical model to consider the macroscopic fault motion obeying the concerned brittle-ductile mixed property (Figure 1c). As illustrated in Figure 3a, we take a standard approach to simply model the average movement of the finite fault area in a "macroscopic" viewpoint [*Bos and Spiers*, 2002; *Daub et al.*, 2011; *Scholz*, 1998]: the one degree-of-freedom system with the parallel connection of the spring-slider and the dashpot (Figure 3b) to incorporate the mixture of brittle (light grey) and ductile (dark grey) fault zone rheology as previously done [*Daub et al.*, 2011]. Here, we introduce the parameter called the brittle fraction R_b to describe "microscopic" characteristics on the fault as the fraction of the area occupied by the brittle patches over a fault area; R_b plays a major role to describe the temperature dependence as described in the following section. Our model describes the fault strength solely by the frictional slider at the brittle limit ($R_b = 1$) and by the dashpot at the ductile limit ($R_b = 0$), and by both within the transitional regime ($0 < R_b < 1$). The equation of motion (EoM) for this model is described by $m\ddot{u}(t) = -k\{u(t) + V_{pl}t + f\{\dot{u}(t)\}$ with the rheological strength

$$f(\dot{u}) = \begin{cases} f_s(R_b) & if\ \dot{u} = 0\ \text{(stick)} \quad (1a) \\ \alpha(R_b)|\dot{u}|^{1/n} + f_d(R_b) & if\ \dot{u} \neq 0\ \text{(slip)}, \quad (2b) \end{cases}$$

where $u(t)$ denotes the displacement at time t with the dot denoting the temporal derivative, m the mass, k the spring constant, V_{pl} the tectonic loading rate. The ductile strength is characterized by α (velocity-strengthening ratio) and the constants n (stress exponent). The brittle strength is simply described by the static friction f_s and the sliding friction f_d $(< f_s)$, and we ignore the secondary transition process from f_s to f_d. Additionally, while we simplify the model by the fully rigid block, the case when the block deforms ductilely is discussed in Supplementary discussion B.

2.3 Time-dependent solution

Before detailing the temperature dependence, for a demonstration purpose, the EoM is analytically solved assuming $n = 1$and $V_{pl} = 0$ with the initial condition $\dot{u}(0) = 0$ and $u(0) = f_s/k$, which corresponds to a slip event occurring when the tectonic load attained the static frictional strength f_s. The particular solution for the slip (the displacement of the spring) is given by the well-known dumped oscillator solution:

$$u(t) = \exp(-\gamma\omega t)\{(1 + \gamma/\xi)\exp(\omega\xi t) + (1 - \gamma/\xi)\exp(-\omega\xi t)\}(f_s - f_d)/(2k)$$

with $\gamma = \alpha/(2\sqrt{mk})$, $\xi = \sqrt{\gamma^2 - 1}$ and $\omega = \sqrt{k/m}$. As plotted in Figure 3c, the solution varies with the damping coefficient γ from the oscillatory if $0 < \gamma < 1$ (under damping), monotonic if $\gamma \geq 1$ (over damping), to the non-inertia limit if $\gamma \gg 1$. Because slow earthquakes are closer to the non-inertia (aseismic) regime, hereafter, we examine the solution for $\gamma \gg 1$, reduced to

$$u(t) = (\max u)\exp(-kt/\alpha) \text{ with } \max u = (f_s - f_d)/k$$

and

$$\dot{u}(t) = (\max \dot{u})\exp(-kt/\alpha) \text{ with } \max \dot{u} = (f_s - f_d)/\alpha.$$

Besides, the non-Newtonian creep case ($n > 1$) exhibits qualitatively the same manner (see Supplementary discussion A). We will see next that the prefactors or the maximum amounts of the slip and slip rate, denoted by $\max u$ and $\max \dot{u}$, essentially involve the temperature effect collectively.

2.4 Temperature-dependent rheology

We incorporate the ambient temperature dependencies in the above strength parameters. First, plastic flows are considered to describe ductility. The rock viscosity η is generally described by the Arrhenius-type temperature dependence [*Karato,* 2008]

$$\eta(T) = \eta_o \exp(H/RT) \sim \eta_o \exp(gT_m/T) \quad (2)$$

with the absolute temperature T, the activation enthalpy H, the gas constant R, the melting temperature T_m and a constant η_o. The detailed dependence of η_o on the grain sizes and the fugacity [*Karato*, 2008] are irrelevant to the qualitative behavior of the system and are discarded in the current analysis. The pressure (P) dependence of the viscosity is much weaker than that of temperature and is indirectly considered in the model through the pressure dependence of $H(P)$ and $T_m(P)$[*Karato*, 2008]. Experiments show that the constant g is of the order of ten[*Karato*, 2008; *Rutter and Brodie*, 2004], and T_m is related to the onset temperature of plasticity as $T_m = g'T_p$ with g' being severalfold for rocks [*Scholz*, 2019].

The temperature dependence of the brittle fraction $R_b(T)$ can be constrained by the geodetic estimate of the interpolate coupling coefficient, which is determined by the area of the locked (i.e., brittle) patches over the otherwise steady sliding areas. Geodetic

observations generally show that the coupling coefficients gradually decrease and moderately change with increasing depth or temperature, as illustrated in Figure 1a [*Avouac*, 2015; *Burgmann*, 2018]. Seismological observations also show a similar tendency for rupture areas to become smaller for deeper earthquakes [*Lay et al.*, 2012]. To model these gradual changes generically, we take a simple approach, assuming several types of functional forms (Figure 4a) and test the robustness of the outcome; such functions should satisfy the condition of the abovementioned monotonic decrease within the transition zone from $R_b(T_{fb}) = 1$ to $R_b(T_{fp}) = 0$ for $T_{fb} < T < T_{fp}$, where T_{fb} and T_{fp} respectively indicate the temperatures at the base of the fully brittle seismogenic zone and the top of the fully plastic aseismic zone. Typical examples of such functions may be given by

$$R_b(T) = \begin{cases} 1 - \{(T - T_{fb})/(T_{fp} - T_{fb})\}^c & for\ T_{fb} < T < T_{fp} \\ Step(T), \end{cases} \quad (3)$$

where c is a constant and $Step(T)$ is a multi-step function plotted in Figure 4a. The multi-step function is hypothesized to mimic sudden changes due to some phase transitions.

2.5 Connecting temperature-dependent rheology with mechanical model parameters

The effects of the ambient temperature T are considered time-independent and are included in the above "macroscopic" strength parameters: $f_s(T) - f_d(T)$ and $\alpha(T)$. We introduce a constant for the force drop, Δf_o, corresponding to the value to be attained at the fully brittle case ($R_b = 1$). Similarly, for the ductile strength when fully ductile, we introduce the velocity-strengthening ratio $\alpha_o(T)(\equiv \eta(T) \times D/w$ with the fault dimension D and fault zone width w.) We do not explicitly concern about the effect of the fault zone width w increasing as going deeper [*Scholz*, 2019] because this effect is merely further decrease η_v together with the temperature dependent decrease of η. In analogy with the real contact area, these parameters constitute the macroscopic strength parameters with the brittle fraction $R_b(T)$ as the function of temperature in the brittle-ductile transitional regime, given by

$$f_s(T) - f_d(T) = R_b(T)\Delta f_o$$

for the brittle strength and, representing the otherwise ductile area,

$$\alpha(T) = [1 - R_b(T)]\alpha_o(T)$$

for the ductile strength, as illustrated in Figures 1c and 3a.

3 Results

3.1 General temperature dependence of slip modes

We are interested in the final slip $\max u$ and the maximum slip rate $\max \dot{u}$ during a single slip event occurring under the ambient temperature T. By considering the above-described temperature-dependent parameters and the temperature-independent rigidity k, it is given by

$$\max u(T) \propto f_s(T) - f_d(T) = \Delta f_o\left[1 - \left\{\left(T - T_{fb}\right)/\left(T_p - T_{fb}\right)\right\}^c\right] \quad (4)$$

and

$$\max \dot{u}(T) \propto \frac{f_s(T) - f_d(T)}{\alpha(T)} = \frac{\Delta f_o\left[1 - \left\{\left(T - T_{fb}\right)/\left(T_p - T_{fb}\right)\right\}^c\right]}{\eta_o\left\{\left(T - T_{fb}\right)/\left(T_p - T_{fb}\right)\right\}^c \exp(gT_m/T)}. \quad (5)$$

Figure 4b plots the viscosity for the dashpot as the function of temperature, exhibiting the extremely rapid reduction attributed to the Arrhenius law. Figure 4c shows the obtained temperature dependence of the force drop or final slip amount (Equation 4). The force drop and slip are merely proportional to $R_b(T)$ because the temperature dependence only appears through the brittle fraction $R_b(T)$. The force drop and slip are decreased as the function of temperature toward T_{fp} as intuitively understood.

3.2 SIL: Seismogenic peak at an intermediate temperature in the deep transition zone

Figure 4d shows the slip rate (Equation 5), which becomes influenced by the temperature dependence of η via α. The remarkable feature presented here is that the prominent peak appears at an intermediate temperature. This peak of the slip rate may not be intuitive. However, this simply manifests the decreasing viscosity as increasing temperature because the smaller viscous resistance leads to faster slip. The brittle fraction $R_b(T)$ and slip tend to decrease as well, but their decrease is much gentler and bounded $0 < R_b(T) < 1$. Such a gentle temperature dependence is easily overcome by the more rapid reduction of the viscosity due to the Arrhenius-type dependence, $\exp(1/T)$ (Figure 4b). (This mechanism is also the reason for a subtle peak at a lower temperature in the multi-step function case because the greater viscosity damps the motion at the first peak.) In other words, such a peak or SIL should exist as long as the viscosity is described by rapidly changing functions like the Arrhenius law.

It is further shown in Figure 4d that the existence of the peak at the intermediate temperature $\left(T_{fb} < T < T_{fp}\right)$ is independent of the assumed functional form of $R_b(T)$.

Further, if $c = 1$ in Equation 3, the peak slip rate always appears at the intermediate temperature T_{sr} given by

$$T_{sr} = \left\{ (T_{fb} + T_p)/2 + \sqrt{(T_p - T_{fb})^2/4 - T_p^2 T_{fb}/gT_m} \right\} / (1 + T_p/gT_m) \quad (6)$$

with the inequality $T_{fb} < T_{sr} < T_p < gT_m$ (detailed in Supplementary material C). This equation predicts that T_{sr} appears somewhat below the temperature of full plasticity, T_{fp}. Additionally, across the trough from the peak, the slip rate in Figure 4d tends to exhibit a rapid increase as the temperature decreases down to the base of the seismogenic zone, T_{fb}, since the ductile strength is to vanish there.

4. Discussions

4.1 Comparison with geophysical observations of deep slow earthquakes

Our analysis results demonstrate that the stress drop (force drop divided by fault area) and the slip decrease with increasing temperature or depth, coinciding with the observed characteristics (Figure 1a). Furthermore, under the constant loading rate, the frequency of events also becomes higher as increasing depth due to the smaller stress drop there. These features can naturally explain the observed small stress drop of the slow earthquakes [*Ide et al.*, 2007; *Miyazaki et al.*, 2006] together with the relatively larger stress drop and longer intervals of L-SSEs than those of S-SSEs [*Frank et al.*, 2015; *Hirose and Obara*, 2005; *Miyazaki et al.*, 2006] (Figure 1). Further, the simulated velocity reproduces the observed peak at an intermediate temperature or depth seen as SIL. Besides, the sliding event could appear steady for the lower temperature side due to the smaller slip rate caused by larger viscosity; this situation perhaps explains the absence of or unfound L-SSEs in Cascadia or San Andreas.

4.2 Implications for rheological mechanisms of shallow-slow earthquakes

Slow earthquakes are also observed in a shallow transition zone above the seismogenic zone [*Ito and Obara*, 2006; *Obara*, 2011; *Obara et al.*, 2010]. While their depth dependences are yet to be established, SIL has not been found even in one of the best-observed subduction zone, Nankai trough, with ocean-bottom sensors thus far [*Araki et al.*, 2017; *Nakano et al.*, 2018]. It may be worth discussing the implication of the current model. The velocity-strengthening friction of clays is proposed to underlie shallow-slow earthquakes [*Saffer and Marone*, 2003] through positive values of the nominal velocity sensitivity factor $A \equiv (a - b)\sigma_n$, where $(a - b)$ and σ_n denote the rate- and state-

dependent frictional parameter and the effective normal stress. Based on the laboratory experiments at a low-temperature regime, they infer A to be a weakly decreasing function or independent of the depth toward the top of the fully-brittle depth D_{fb}, as simply represented by the red and blue lines in Figure 4f, respectively, without loss of generality.

To explore the mechanism of the shallow events, we assume the depth-dependence similarly to the temperature-dependence of the deep ones but incorporate the abovementioned depth-dependence of the rate-dependent friction at a low-temperature regime (detailed in Supplementary method D). The depth D dependence of the parameters A and R_b are taken in general power-law forms respectively as a decreasing function $A(D) = A_o\{1 - (D/D_{fb})^{c_1}\}$ with constants $A_o > 0$ and $c_1 \geq 0$ (Figure 4f) and as an increasing function $R_b(D) = (D/D_{fb})^{c_2}$ with a constant $c_2 > 0$ (Figure 4e). Following the same algebra, we obtained the expressions as $\max u(D) \propto \Delta f(D/D_{fb})^{c_2}$ and $\max \dot{u}(D) \propto \Delta f_o(D/D_{fb})^{c_2}/[A_o\{1 - (D/D_{fb})^{c_2}\}\{1 - (D/D_{fb})^{c_1}\}]$. As exemplified for $c_1 = 0\ and\ 1$ with $c_2 = 1$ (Figure 4i-h), the calculated slip rate is increased monotonically up to the fully brittle depth (Figure 4h). This trend is simply because the brittle fraction increases while the ductile strength vanishes with increasing depth. This result seems to match the observation of the absence of SIL for the shallow transition zone.

4.3 Implications for physics-based models of deep-slow earthquakes

The temperature dependence of the velocity-strengthening friction further contributes to identifying the origin of the ductility controlling slow earthquakes in the deep transition zone. In a high-temperature regime, laboratory experiments [*Blanpied et al.*, 1995; *den Hartog et al.*, 2012; *Okamoto et al.*, 2019] show that the velocity-strengthening friction tends to increase the sensitivity to the velocity with increasing temperature, as shown in Figure 1b and simplified in Figure 4j (blue line). The consequence of this tendency, along with the reduction of R_b (Figure 4i), gives the symmetric patterns with the shallow case (Figure 4e-h), obtained simply by flipping and replacing D with T. The setup of $(a - b)$ in the blue line case (Figure 4f and j) is qualitatively the same as those of the common in the rate- and state-dependent fault models for both the shallow and deep sides [e.g., *Tse and Rice*, 1986]. As a result, the slip amount shows the monotonic decrease as increasing temperature (Figure 4k), similarly to the plasticity case (Figure 4c). We further observe the monotonic decrease of the slip rate

as increasing temperature without exhibiting SIL (Figure 4l). The latter clearly shows the different outcomes from the current knowledge in the temperature dependences of the plastic creep and the rate-dependent friction.

Regarding the reproducibility of SIL, we preferer the deep-slow earthquake models with the plastic flow mechanisms together with brittle-ductile heterogeneities [e.g., *Ando et al.*, 2012; *Beall et al.*, 2019] rather than any models incorporating the rate-dependence of friction. The application of the rate- and state-dependent friction should work in determining the base of the seismogenic zone due to the overall velocity-weakening to strengthening transition [e.g., *Noda and Shimamoto*, 2012; *Scholz*, 2019]. However, this application in the macroscopic viewpoint (that homogenizes the rock heterogeneity) predicts a monotonic change from the fully seismic (fast slip) to aseismic regimes along the depth via the slow slip regime associated with the neutral stability mechanism [e.g., *Liu and Rice*, 2007]. Thus, the physics-based models in this line of thinking will be insufficient to explain the presence of SIL. Additional microscopic factors will be needed, which naturally arise from the internal heterogeneity of fault rock rheology emerging at the transitional P-T condition.

5 Conclusion

We develop a simple physics-based model of slow earthquakes that incorporates the temperature dependence of rock rheology in the brittle-ductile transitional regime. Geological observations of the plastically-deformed matrix and competent blocks in mineralogically heterogeneous fault zones are mimicked. Our model naturally reproduces the seismogenic inversion layer (SIL) without finely tuning rheological parameters. The key mechanism is the reduction in both the fraction of brittle blocks and the viscosity of the matrix with increasing temperature/depth independent of tectonic settings.

Acknowledgment

This work is supported in part by KAKENHI 18KK0095, 19H04622, 20KK0078, JP21H05203 and 22H05300.

Open research

Data is available through Ujiie et al., 2022 and Tulley et al., 2022.

Author contributions

R. A. designed the project, developed the mechanical model, conducted the analysis and wrote the manuscript. K. U., N. N. and Y. M. conducted the field survey and developed the geological interpretations. All authors discuss the results and contribute to the writing.

Competing interest statement

The authors declare no competing interests.

References

Ando, R., N. Takeda, and T. Yamashita (2012), Propagation dynamics of seismic and aseismic slip governed by fault heterogeneity and Newtonian rheology, *J. Geophys. Res.*, *117*, B11308, doi:10.1029/2012jb009532.

Araki, E., D. M. Saffer, A. J. Kopf, L. M. Wallace, T. Kimura, Y. Machida, S. Ide, E. Davis, and E. S. Scientist (2017), Recurring and triggered slow-slip events near the trench at the Nankai Trough subduction megathrust, *Science*, *356*(6343), 1157-1160, doi:10.1126/science.aan3120.

Audet, P., M. G. Bostock, N. I. Christensen, and S. M. Peacock (2009), Seismic evidence for overpressured subducted oceanic crust and megathrust fault sealing, *Nature*, *457*(7225), 76-78.

Avouac, J. P. (2015), From Geodetic Imaging of Seismic and Aseismic Fault Slip to Dynamic Modeling of the Seismic Cycle, *Annual Review of Earth and Planetary Sciences, Vol 43*, *43*, 233-271, doi:10.1146/annurev-earth-060614-105302.

Beall, A., A. Fagereng, and S. Ellis (2019), Fracture and Weakening of Jammed Subduction Shear Zones, Leading to the Generation of Slow Slip Events, *Geochem. Geophys. Geosyst.*, *20*(11), 4869-4884, doi:10.1029/2019gc008481.

Behr, W. M., A. J. Kotowski, and K. T. Ashley (2018), Dehydration-induced rheological heterogeneity and the deep tremor source in warm subduction zones, *Geology*, *46*(5), 475-478, doi:10.1130/G40105.1.

Blanpied, M. L., D. A. Lockner, and J. D. Byerlee (1995), Frictional Slip of Granite at Hydrothermal Conditions, *J. Geophys. Res.*, *100*(B7), 13045-13064, doi:Doi 10.1029/95jb00862.

Bos, B., and C. J. Spiers (2002), Frictional-viscous flow of phyllosilicate-bearing fault rock:

414 Microphysical model and implications for crustal strength profiles, *J. Geophys. Res.*, *107*(B2),
415 doi:10.1029/2001jb000301.
416 Boyer, F., E. Guazzelli, and O. Pouliquen (2011), Unifying Suspension and Granular Rheology,
417 *Phys. Rev. Lett.*, *107*(18), doi:10.1103/PhysRevLett.107.188301.
418 Burgmann, R. (2018), The geophysics, geology and mechanics of slow fault slip, *Earth Planet*
419 *Sc Lett*, *495*, 112-134, doi:10.1016/j.epsl.2018.04.062.
420 Currie, C. A., R. D. Hyndman, K. Wang, and V. Kostoglodov (2002), Thermal models of the
421 Mexico subduction zone: Implications for the megathrust seismogenic zone, *J. Geophys. Res.*,
422 *107*(B12), doi:10.1029/2001jb000886.
423 Daub, E. G., D. R. Shelly, R. A. Guyer, and P. A. Johnson (2011), Brittle and ductile friction
424 and the physics of tectonic tremor, *Geophys. Res. Lett.*, *38*, L10301,
425 doi:10.1029/2011GL046866.
426 den Hartog, S. A. M., A. R. Niemeijer, and C. J. Spiers (2012), New constraints on megathrust
427 slip stability under subduction zone P-T conditions, *Earth Planet Sc Lett*, *353*, 240-252,
428 doi:10.1016/j.epsl.2012.08.022.
429 Fagereng, A., G. W. B. Hillary, and J. F. A. Diener (2014), Brittle-viscous deformation, slow
430 slip, and tremor, *Geophys. Res. Lett.*, *41*(12), 4159-4167.
431 Frank, W. B., M. Radiguet, B. Rousset, N. M. Shapiro, A. L. Husker, V. Kostoglodov, N. Cotte,
432 and M. Campillo (2015), Uncovering the geodetic signature of silent slip through repeating
433 earthquakes, *Geophys. Res. Lett.*, *42*(8), 2774-2779, doi:10.1002/2015gl063685.
434 Hacker, B. R., G. A. Abers, and S. M. Peacock (2003), Subduction factory - 1. Theoretical
435 mineralogy, densities, seismic wave speeds, and H2O contents, *J. Geophys. Res.*, *108*(B1),
436 doi:10.1029/2001JB001127.
437 Hirose, H., and K. Obara (2005), Repeating short- and long-term slow slip events with deep
438 tremor activity around the Bungo channel region, southwest Japan, *Earth Planets Space*,
439 *57*(10), 961-972.
440 Howell, D., R. P. Behringer, and C. Veje (1999), Stress fluctuations in a 2D granular Couette
441 experiment: A continuous transition, *Phys. Rev. Lett.*, *82*(26), 5241-5244,
442 doi:10.1103/PhysRevLett.82.5241.
443 Hyndman, R. D., P. A. McCrory, A. Wech, H. Kao, and J. Ague (2015), Cascadia subducting
444 plate fluids channelled to fore-arc mantle corner: ETS and silica deposition, *J. Geophys. Res.*,
445 *120*(6), 4344-4358, doi:10.1002/2015jb011920.
446 Ide, S., G. C. Beroza, D. R. Shelly, and T. Uchide (2007), A scaling law for slow earthquakes,
447 *Nature*, *447*(7140), 76-79.
448 Ito, Y., and K. Obara (2006), Very low frequency earthquakes within accretionary prisms are
449 very low stress-drop earthquakes, *Geophys. Res. Lett.*, *33*(9), doi:10.1029/2006gl025883.

Karato, S. I. (2008), Deformation of Earth Materials: An Introduction to the Rheology of Solid Earth, *Deformation of Earth Materials: An Introduction to the Rheology of Solid Earth*, 1-463, doi:10.1017/Cbo9780511804892.

Katayama, I., T. Terada, K. Okazaki, and A. Tanikawa (2012), Episodic tremor and slow slip potentially linked to permeability contrasts at the Moho, *Nat Geosci*, *5*(10), 731-734, doi:10.1038/Ngeo1559.

Kobayashi, A. (2017), Objective detection of long-term slow slip events along the Nankai Trough using GNSS data (1996-2016), *Earth Planets Space*, *69*, doi:10.1186/s40623-017-0755-7.

Lay, T., H. Kanamori, C. J. Ammon, K. D. Koper, A. R. Hutko, L. L. Ye, H. Yue, and T. M. Rushing (2012), Depth-varying rupture properties of subduction zone megathrust faults, *J. Geophys. Res.*, *117*, doi:10.1029/2011JB009133.

Liu, Y. J., and J. R. Rice (2007), Spontaneous and triggered aseismic deformation transients in a subduction fault model, *J. Geophys. Res.*, *112*(B9), B09404, doi:doi:10.1029/2007JB004930.

Matsuzawa, T., B. Shibazaki, K. Obara, and H. Hirose (2013), Comprehensive model of short- and long-term slow slip events in the Shikoku region of Japan, incorporating a realistic plate configuration, *Geophys. Res. Lett.*, *40*(19), 5125-5130, doi:10.1002/grl.51006.

Michel, S., A. Gualandi, and J. P. Avouac (2019), Interseismic Coupling and Slow Slip Events on the Cascadia Megathrust, *Pure Appl. Geophys.*, *176*(9), 3867-3891, doi:10.1007/s00024-018-1991-x.

Miyazaki, S., P. Segall, J. J. McGuire, T. Kato, and Y. Hatanaka (2006), Spatial and temporal evolution of stress and slip rate during the 2000 Tokai slow earthquake, *J. Geophys. Res.*, *111*(B3), doi: 10.1029/2004JB003426

Mori, Y., M. Shigeno, and T. Nishiyama (2014), Fluid-metapelite interaction in an ultramafic melange: implications for mass transfer along the slab-mantle interface in subduction zones, *Earth Planets Space*, *66*, doi:10.1186/1880-5981-66-47.

Nakano, M., T. Hori, E. Araki, S. Kodaira, and S. Ide (2018), Shallow very-low-frequency earthquakes accompany slow slip events in the Nankai subduction zone, *Nat Commun*, *9*, doi:ARTN 984

10.1038/s41467-018-03431-5.

Nishiyama, T. (1989), Petrologic study of the Nagasaki metamorphic rocks in the Nishisonogi peninsula–with special reference to the greenrock complex and the reaction-enhanced ductility, *Mem. Geol. Soc. Japan*, *33*, 237-257.

Nishiyama, T. (1990), CO2-metasomatism of a metabasite block in a serpentine melange from the Nishisonogi metamorphic rocks, southwest Japan, *Contributions to Mineralogy and*

Petrology, *104*(1), 35-46, doi:10.1007/BF00310644.
Noda, H., and T. Shimamoto (2012), Transient behavior and stability analyses of halite shear zones with an empirical rate-and-state friction to flow law, *J. Struct. Geol.*, *38*, 234-242, doi:10.1016/j.jsg.2011.08.012.
Obara, K. (2011), Characteristics and interactions between non-volcanic tremor and related slow earthquakes in the Nankai subduction zone, southwest Japan, *J Geodyn*, *52*(3-4), 229-248, doi:10.1016/j.jog.2011.04.002.
Obara, K., S. Tanaka, T. Maeda, and T. Matsuzawa (2010), Depth-dependent activity of non-volcanic tremor in southwest Japan, *Geophys. Res. Lett.*, *37*, doi:10.1029/2010gl043679.
Okamoto, A. S., B. A. Verberne, A. R. Niemeijer, M. Takahashi, I. Shimizu, T. Ueda, and C. J. Spiers (2019), Frictional Properties of Simulated Chlorite Gouge at Hydrothermal Conditions: Implications for Subduction Megathrusts, *J. Geophys. Res.*, *124*(5), 4545-4565, doi:10.1029/2018jb017205.
Peacock, S. M. (2009), Thermal and metamorphic environment of subduction zone episodic tremor and slip, *J. Geophys. Res.*, *114*, B00A07, doi:doi: 10.1029/2008JB005978.
Rogers, G., and H. Dragert (2003), Episodic tremor and slip on the Cascadia subduction zone: The chatter of silent slip, *Science*, *300*(5627), 1942-1943.
Rutter, E. H., and K. H. Brodie (2004), Experimental intracrystalline plastic flow in hot-pressed synthetic quartzite prepared from Brazilian quartz crystals, *J. Struct. Geol.*, *26*(2), 259-270, doi:10.1016/S0191-8141(03)00096-8.
Saffer, D. M., and C. Marone (2003), Comparison of smectite- and illite-rich gouge frictional properties: application to the updip limit of the seismogenic zone along subduction megathrusts, *Earth Planet Sc Lett*, *215*(1-2), 219-235, doi:10.1016/S0012-821x(03)00424-2.
Scholz, C. H. (1998), Earthquakes and friction laws, *Nature*, *391*(6662), 37-42.
Scholz, C. H. (2019), *The Mechanics of Earthquakes and Faulting*, 3rd ed., Cambridge Univ. Press, Cambridge, United Kingdom, doi:10.1017/9781316681473.
Segall, P., A. M. Rubin, A. M. Bradley, and J. R. Rice (2010), Dilatant strengthening as a mechanism for slow slip events, *J. Geophys. Res.*, *115*, B12305, doi:10.1029/2010JB007449.
Shelly, D. R., and K. M. Johnson (2011), Tremor reveals stress shadowing, deep postseismic creep, and depth-dependent slip recurrence on the lower-crustal San Andreas fault near Parkfield, *Geophys. Res. Lett.*, *38*, doi:10.1029/2011gl047863.
Sibson, R. H. (1977), Fault rocks and fault mechanisms, *J. Geol. Soc. Lond.*, *133*(Part 3), 191-213.
Skarbek, R. M., A. W. Rempel, and D. A. Schmidt (2012), Geologic heterogeneity can produce aseismic slip transients, *Geophys. Res. Lett.*, *39*, doi:10.1029/2012gl053762.
Tse, S. T., and J. R. Rice (1986), Crustal Earthquake Instability in Relation to the Depth

522 Variation of Frictional Slip Properties, *J. Geophys. Res.*, *91*(B9), 9452-9472.
523 Tulley, C. J., A. Fagereng, K. Ujiie, J. F. A. Diener, and C. Harris (2022), Embrittlement
524 Within Viscous Shear Zones Across the Base of the Subduction Thrust Seismogenic Zone,
525 *Geochem. Geophys. Geosyst.*, *23*(9), doi:ARTN e2021GC010208
526 10.1029/2021GC010208.
527 Ujiie, K., K. Noro, N. Shigematsu, Å. Fagereng, N. Nishiyama, C. J. Tulley, H. Masuyama, Y.
528 Mori, and H. Kagi (2022), Megathrust Shear Modulated by Albite Metasomatism in
529 Subduction Mélanges, *Geochemistry, Geophysics, Geosystems*, *23*(8), e2022GC010569,
530 doi:https://doi.org/10.1029/2022GC010569.
531 Ujiie, K., H. Saishu, A. Fagereng, N. Nishiyama, M. Otsubo, H. Masuyama, and H. Kagi
532 (2018), An Explanation of Episodic Tremor and Slow Slip Constrained by Crack-Seal Veins
533 and Viscous Shear in Subduction Melange, *Geophys. Res. Lett.*, *45*(11), 5371-5379,
534 doi:10.1029/2018gl078374.
535 Wech, A. G., C. M. Boese, T. A. Stern, and J. Townend (2012), Tectonic tremor and deep slow
536 slip on the Alpine Fault, *Geophys. Res. Lett.*, *39*, doi:10.1029/2012gl051751.
537 Wech, A. G., K. C. Creager, and T. I. Melbourne (2009), Seismic and geodetic constraints on
538 Cascadia slow slip, *J. Geophys. Res.*, *114*, doi:10.1029/2008JB006090.
539 Zhu, L. P. (2000), Crustal structure across the San Andreas Fault, southern California from
540 teleseismic converted waves, *Earth Planet Sc Lett*, *179*(1), 183-190, doi:Doi 10.1016/S0012-
541 821x(00)00101-1.
542
543
544

Figures, table and captions

Table 1. Observation-based characterization of depth-dependent modes of deep-slow earthquakes and host rock materials* from typical plate-interface examples.

	Subduction interfaces		Transform interfaces
	Nankai / Guerrero	Cascadia	San Andreas / Alpine
Shallow Cold	Regular earthquakes		
	Crust		
Shallower Colder	Long-term SSEs with no or little tremor [*Frank et al.*, 2015; *Kobayashi*, 2017]	No ETS found but not fully coupled [*Hyndman et al.*, 2015; *Michel et al.*, 2019]	No tremor found [*Shelly and Johnson*, 2011; *Wech et al.*, 2012]
	Crust	Crust	Crust
Deeper Warmer	Short-term SSEs with tremor or ETS [*Obara*, 2011]	SSEs with tremor (ETS). Shallower peak of Slip than that of tremor[*Wech et al.*, 2009]	Episodic tremor with possible episodic slip [*Shelly and Johnson*, 2011; *Wech et al.*, 2012]
	Mantle [*Obara*, 2011] / At Moho [*Currie et al.*, 2002]	Crust with unclear Moho [*Audet et al.*, 2009]	Crust [*Zhu*, 2000] / Mostly in lower crust [*Wech et al.*, 2012]
Deep Warm	Stable sliding		
	Mantle		

*Upper plate materials are indicated for subduction zones.

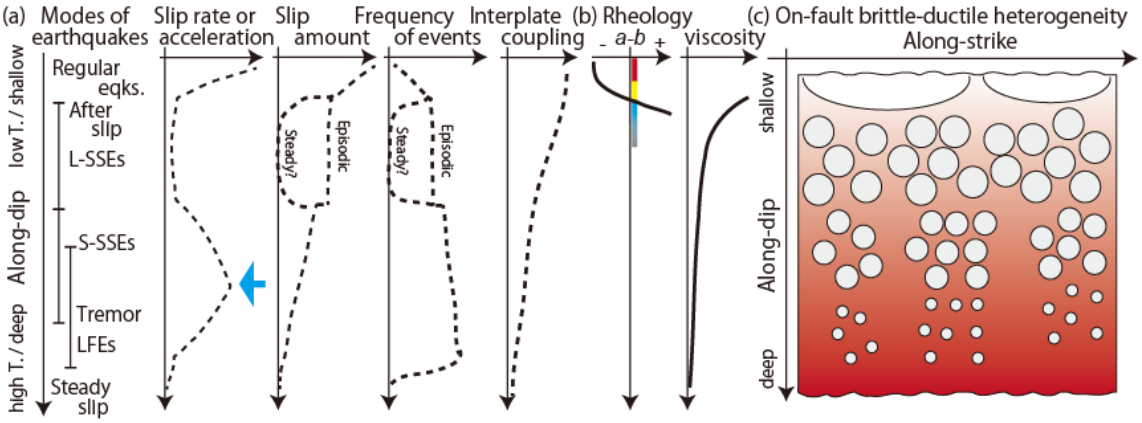

Figure1. Depth-dependent characteristics of deep slow earthquakes and fault rheology around the brittle-ductile transition depth. (a) Schematic diagrams of observed depth dependences of the parameters for individual slow earthquake events and the interplate coupling condition [*Avouac*, 2015; *Burgmann*, 2018]. The depth ranges and the modes of slow earthquakes are characterized as indicated; L-SSEs: Long-term slow slip events. S-SSEs: Short-term SSEs. LFEs: Low-frequency earthquakes. The blue arrow points to the peak in the seismogenic inversion layer (SIL). (b) Rheological properties on the slip velocity dependence coefficient $(a - b)$ of the rate- and state-friction (RSF) and the plastic flow viscosity. The colors along the vertical axis indicate the RSF regimes [*Scholz*, 1998] of unstable (red), conditionally stable (yellow), and stable (blue). (c) Schematics of the heterogeneous distribution of the rheological properties on a fault surface. The circles represent the brittle patches existing on the surrounding ductile background. The patch sizes/density and the background viscosity (indicated by the graded color) are decreasing functions of the depth.

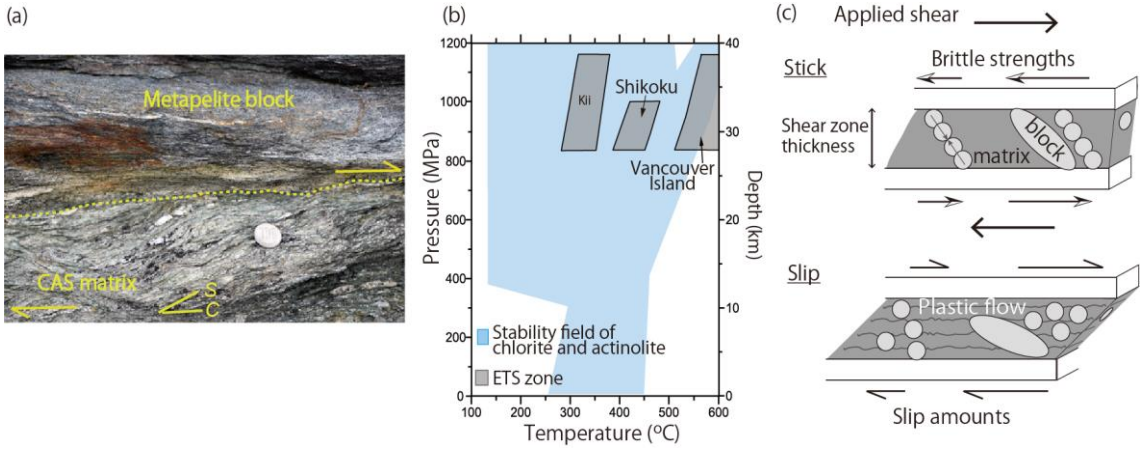

Figure 2. Internal material structure and deformation pattern of a fault zone. (a) Geologically observed block-in-matrix structure. Metapelite blocks surrounded by chlorite-actinolite schist (CAS) matrix. The arrows and lines respectively indicate the estimated shear sense and S-C fabrics. Outcrop examples in Nishikashiyama mélange, southwest Japan. (b) The P-T conditions for the stability field of chlorite and actinolite (redrawn from the facies of prehnite-actinolite, greenschist, epidote amphibolite, epidote-garnet amphibolite, lawsonite blueschist, jadeite lawsonite blueschist and epidote blueschist) [*Hacker et al.*, 2003] and the ETS zones in Nankai (Kii and Shikoku) and Cascadia (Vancouver island) subductions zones [*Peacock*, 2009]. (c) Schematics of fault zone motion. For the stick period (upper), the applied shear stress is resisted by the engaged brittle blocks with the stress chains. The denser distribution of blocks has a larger brittle strength. During a slip event (lower), the depinning due to the collapse and rotation of blocks release the shear stress slowly by the matrix plastic flows. The blocks are rearranged, forming force chains to be stuck again, recurring the stick-slip motion.

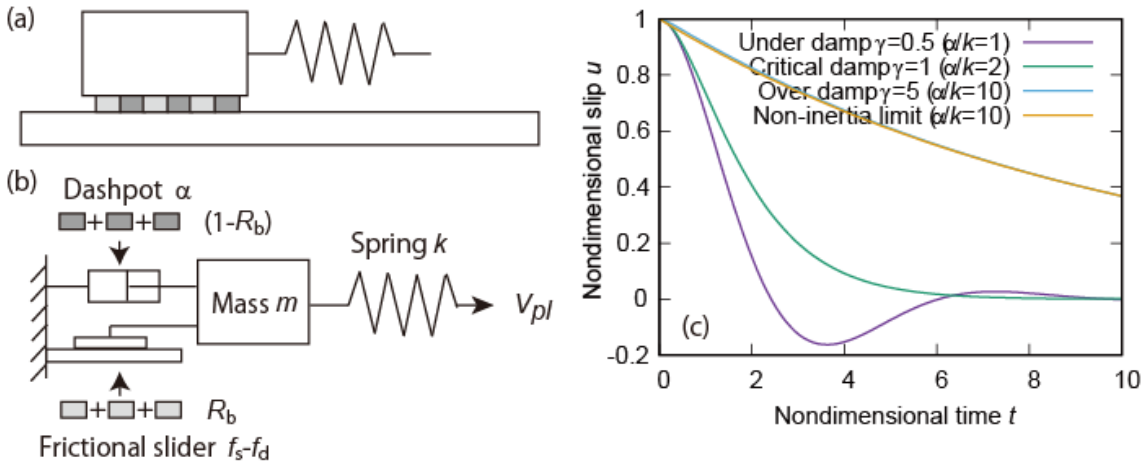

Figure 3. One degree of freedom model for a brittle-ductile heterogeneous fault. (a) The gross interfacial rheology determined by brittle areas with the brittle fraction R_b (light grey) and otherwise ductile areas (dark grey). (b) The modeling elements consisting of the dashpot and the slider, respectively representing the ductile and brittle sections in (a), which are connected in parallel to the mass and the spring. (c) Temporal progress of the block displacement (slip) for various values of the damping coefficient γ.

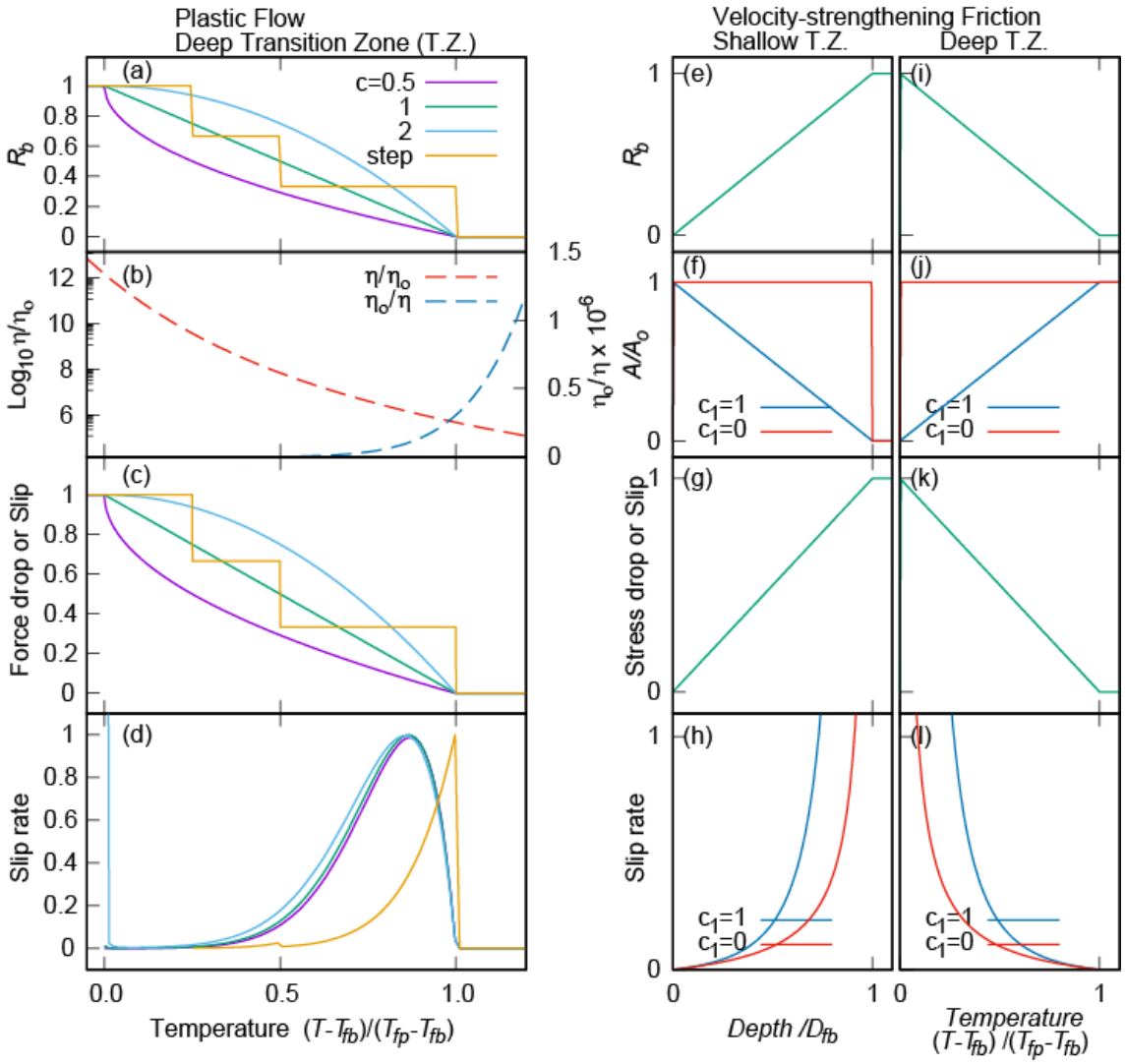

Figure 4. Model conditions and simulated sliding characteristics as the function of the temperature. The horizontal axis, $T - T_{fb}$, indicates the temperature measured from the base of the fully brittle zone (T_{fb}). (a)-(d) The case of plastic flow for the ductility of the deep transition zone. (a) Assumed brittle fraction $R_b(T)$ for different dependences on T as the power-low functions with the exponent $c = 0.5 - 2$ and the multi-step function. (b) Normalized viscosity $\eta/\eta_o = \exp(gT_m/T)$ with $gT_m = 25(T_p - T_{fb})$. (c) Normalized force drop and slip amount. (d) The maximum slip rate. The line colors in (a), (c) and (d) indicate the cases of the same values of c. The cases of the simplified velocity-strengthening friction applied to the shallow (e)-(h) and deep (i)-(l) transition zones. The exponent c_1 discriminates the depth-dependence of the velocity strengthening ratio A (see the main text for explanations). The values in the vertical axes are normalized by the individual peak values in (c), (d), (g) and (k).

612